ELSEVIER
SAUNDERS

Thorac Surg Clin 14 (2004) 25–42

THORACIC
SURGERY
CLINICS

Imaging of the mediastinum: applications for thoracic surgery

Dorith Shaham, MD[a,*], Maria G. Skilakaki, MD[b], Orly Goitein, MD[a]

[a]*Department of Radiology, Hadassah University Hospital, Ein-Kerem, Jerusalem 91120, Israel*
[b]*Department of Radiology, Evangelismos General Hospital, 45–47 Ipsiladou Street, 10675 Athens, Greece*

The mediastinum is a complex anatomic division of the thorax, extending from the thoracic inlet superiorly to the diaphragm inferiorly. The mediastinum is bordered anteriorly by the sternum, posteriorly by the vertebral column, and laterally by the parietal pleura.

The mediastinum is further subdivided into superior, anterior, middle, and posterior divisions. The exact anatomic borders of these divisions are unclear, and different authors have different definitions [1]. Additionally, these borders do not have clear-cut implications to the development of disease and do not form barriers to the spread of disease; however, each compartment of the mediastinum has its own most common lesions, and knowing the location of the mass, the patient's age, and the presence or absence of symptoms considerably narrows the range of possible diagnoses [2,3].

The complex anatomy of the mediastinum is best understood by cross-sectional images provided by CT or MRI.

According to Gray's anatomy [4], the mediastinum is divided into superior and inferior compartments by an imaginary line from the lower border of the manubrium to the lower border of the fourth thoracic vertebra. The anterior mediastinum lies anterior to the pericardium and ascending aorta. The posterior mediastinum is bounded in front by the trachea, the pulmonary vessels, and the pericardium and behind by the vertebral column. The middle mediastinum is bordered anteriorly by the anterior pericardial reflection and posteriorly by the posterior pericardial reflection.

The bulk of the mediastinum is composed of the heart and blood vessels. The carina, major airways, and the esophagus are also identified easily in the normal mediastinum and are surrounded by a variable amount of fatty areolar tissue.

The contents of the anterosuperior mediastinum include the thymus gland, the aortic arch and its branches, the great veins, and the lymphatics. The middle mediastinum contains the heart, pericardium, phrenic nerves, carina and main bronchi, hila, and lymph nodes. The contents of the posterior mediastinum include the esophagus, vagus nerves, sympathetic nervous chain, thoracic duct, descending aorta, azygos and hemiazygos veins, and paravertebral lymph nodes.

Various imaging modalities

Almost half of all mediastinal masses do not produce symptoms and are discovered on imaging examinations obtained for other reasons [2,5,6]. In recent years several developments in radiographic techniques and immunohistochemistry have led to more accurate preoperative delineation and histologic diagnosis of mediastinal lesions. Today the presurgical evaluation of a mediastinal mass often involves an array of imaging modalities and percutaneous or transbronchial biopsy techniques [3,7].

Plain chest radiography

The standard posterior–anterior and lateral chest roentgenogram continue to form the cornerstone of

* Corresponding author.
E-mail address: dshaham@hadassah.org.il (D. Shaham).

1547-4127/04/$ – see front matter
doi:10.1016/S1547-4127(04)00039-8

diagnostic imaging [3]. High kilovoltage techniques [>120 peak kilovoltage (KVp)] have significant advantages over low kilovoltage techniques (~70–90 KVp) for demonstrating mediastinal interfaces and providing better penetration of the mediastinum [6]. In most cases deformation of the mediastinal contours must be present for the radiologist to identify a mass, manifested as focal or widespread displacement of normal structures or of the mediastinal pleura [8]. Other features to be evaluated include lesion shape, margins, location, the presence of single or multifocal masses, the presence and type of calcification (eg, rim-like calcification suggests a cystic or vascular lesion), and associated findings such as pleural involvement [9,10]. Mediastinal masses are typically rounded and well circumscribed with smooth margins. Occasionally they might be inseparable from adjacent mediastinal structures and have an obtuse angle or interface. A poor margin at the pulmonary interface usually indicates invasiveness of the lesion, but the most reliable sign of malignancy is spread of disease [6,11].

Old films, if available, are often helpful. Observation of growth rate, duration, and change in nature of the mass can contribute greatly to diagnostic accuracy and guide further investigation [7,9].

CT

After an initial assessment using plain chest radiography, the next step in radiologic evaluation is CT. CT is extremely valuable in the radiographic evaluation of the mediastinum and might be the only imaging modality needed in the investigation of a mediastinal mass [3,9,10,12–14]. CT is commonly used to define and further characterize a mediastinal abnormality diagnosed on plain chest radiographs. Additionally, CT is also often used to evaluate the mediastinum in patients who have normal chest radiographs but a clinical reason to suspect mediastinal disease [12,14]. CT can depict vascular abnormalities and small masses that do not deform the mediastinal contour on chest radiographs following intravenous administration of contrast material [9].

The attenuation of a mediastinal lesion, as measured in Hounsfield units (HU), allows detection of cysts, fat, soft tissue masses, calcification, and air and is extremely important in the differential diagnosis of mediastinal masses [15–17]. Masses can be categorized according to their attenuation [12].

Fat attenuation

Fat attenuation (−70 to −100 HU) masses include lesions composed primarily of or partially containing fat or lipid-rich tissues. Abnormalities of fat distribution can be diffuse, as in mediastinal lipomatosis, or focal, as in lipoma, thymolipoma, and lipoblastoma. Most fatty masses are seen in the peridiaphragmatic areas, and they most often represent herniation of abdominal fat. As a general rule, the fatty nature of a mediastinal mass is a strong indication toward benignancy [12,17–19].

Low attenuation

Low attenuation (about −20 to +20 HU) masses have a density greater than fat but less than muscle. These masses are usually cystic and include congenital benign cysts (bronchogenic, esophageal duplication, neurenteric, pericardial, and thymic cysts), meningocele, mature cystic teratoma, and lymphangioma. Additionally, many tumors can undergo cystic degeneration, especially after radiation therapy or chemotherapy, and demonstrate mixed solid and cystic components at CT, including thymoma, lymphoma, germ cell tumors, mediastinal carcinoma, metastases to lymph nodes, and nerve root tumors. Sometimes, when degeneration is extensive, such tumors might mimic the appearance of congenital cysts; however, clinical history and other manifestations allow correct diagnosis in most cases. Finally, a mediastinal abscess or pancreatic pseudocyst might also appear as a fluid-containing mediastinal cystic mass [12,14,20–22].

High attenuation

High attenuation masses have a density greater than that of muscle (>60 HU). The high density can be attributed to calcium (calcified lymph nodes, partially calcified primary neoplasms including germ-cell tumors, thymoma, and neurogenic tumors, calcified goiter, calcified vascular lesions) or to the presence of fresh blood in a mediastinal hematoma [12,16].

Enhancement

Enhancing masses show a significant increase in attenuation following the injection of contrast. These lesions are highly vascular and include substernal thyroid, parathyroid glands, carcinoid tumor, paraganglioma, Castleman's disease, lymphangioma, and hemangioma [12,23–26].

In recent years the advent of spiral (helical) CT has fundamentally revised the approach to scanning the mediastinum [12]. Spiral CT data sets coupled with a real-time volume-rendering technique allow creation of accurate three-dimensional images, which, although they are not required for diagnosis, can

aid radiologists and referring clinicians by demonstrating anatomic relationships and the extent of disease. Volume-rendered images can be helpful in assessing chest wall extension and collateral vessels caused by obstruction of the superior vena cava [27]. Spiral CT also allows two-dimensional imaging in various planes, including coronal, sagittal, and various angled planes.

MRI

MRI is used less frequently compared with CT in the evaluation of mediastinal masses, mainly because of its lesser availability and higher cost [3,10,28]; however, MRI has a capacity for multiplanar imaging and the ability to image vessels, and it can provide better tissue characterization than CT. Additionally, MRI is excellent in the evaluation of regions of complex anatomy such as the thoracic inlet, the perihilar, paracardiac, and peridiaphragmatic regions, and for the assessment of posterior mediastinal or paravertebral masses [6,12,29]. MRI has completely replaced myelography for the evaluation of potential spinal involvement of posterior neurogenic tumors [3].

MRI is the primary imaging modality for investigating mediastinal abnormalities that are suspected to be vascular. Additionally, the difference in signal between flowing blood and stationary tissues can be used to demonstrate invasion or narrowing of the large arteries and veins of the mediastinum. In selected cases magnetic resonance angiography can be used to demonstrate vascular disorders and distortion, displacement, or stenosis of vessels by mediastinal masses [6,12,30,31]. Conventional angiography and venography, previously performed routinely in the preoperative assessment of invasive primary mediastinal tumors, are now only occasionally used [7]. Additional indications for MRI include the diagnosis of cystic lesions not of cystic attenuation on CT scans (ie, identification of fluid with high protein content) [9,29] and the differential diagnosis between residual tumor and fibrous tissue in a patient who has lymphoma or carcinoma that has been treated [6,9,12,29].

Ultrasonography

Ultrasonography (US) is not commonly used in the evaluation of mediastinal lesions, but it has been reported as a useful alternative to more costly techniques in the assessment of mediastinal masses in selected cases, especially in children [3,9,10,32]. Transesophageal US has been introduced recently to demonstrate mediastinal lesions adjacent to the esophagus, particularly subcarinal lymph nodes and cysts [33,34].

This method can determine whether or not a lesion is cystic and demonstrate its relationship to adjacent structures. Transesophageal US appears to be the best method to verify if an esophageal impression is intramural or extrinsic to the esophageal wall, thus giving additional information about the origin of a mediastinal cyst [34].

Radionuclide imaging

Radionuclide imaging can be helpful in the differential diagnosis of certain mediastinal lesions. Iodine scanning using iodine-123 or iodine-131 can demonstrate functioning thyroid tissue while scanning with technetium-99m (Tc-99) sestamibi can detect parathyroid tissue [21,35].

Preoperative differentiation between thymoma and thyroid hyperplasia or between recurrent tumor and scar tissue can be facilitated by somatostatin receptor scintigraphy with indium-111-octreotide. Additionally, thallium-201 scintigraphy has been reported to enable distinction between normal thymus, lymphoid follicular hyperplasia, and thymoma in patients who have myasthenia gravis [35–38].

Metaiodobenzylguanidine (a precursor of epinephrine) scans detect pheochromocytomas and neuroblastomas, and Tc-99 pertechnate scans can help identify gastric mucosa in suspected neuroenteric cysts [3,6].

Radionuclide scintigraphy has met with variable success in the assessment of malignant lymphomas over the past 30 years. The appearance of the anterior mediastinum after treatment is quite variable, and neither CT nor MRI has proven to be reliable in excluding the presence of active disease in certain cases. Gallium-67 citrate and thallium-201 scintigraphy have been reported recently as being highly sensitive and specific in the detection of residual or recurrent disease [39,40].

Finally, the role of fluorodeoxyglucose (FDG) positron emission tomography (PET) in the assessment of the extent of malignant mediastinal tumors and its utility for initial staging and for predicting prognosis are under investigation [6,38,41–43], and initial results seem to be promising [38]. Recently, combined PET-CT scanners have been introduced that might further facilitate the diagnosis and follow-up of mediastinal masses.

Differential diagnosis of mediastinal tumors by compartments

Classification of mediastinal masses into anterior, middle, and posterior compartments is a convenient categorization method, although there are no anatomical boundaries that limit the extension of masses from these compartments. In general, the most common mediastinal tumor location is the anterior compartment (50–60% in most series) [44,45]. Anterior mediastinal masses include thymoma, lymphoma, teratoma, and germ cell tumors. The most frequent lesions seen in the middle mediastinum are reactive lymph nodes, bronchogenic cysts, and pleuropericardial cysts. Tumors arising in the posterior mediastinum tend to be neurogenic in origin (Box 1) [3,20,36].

Box 1. Classification of the most frequent mediastinal masses according to their typical location

Anterior mediastinal masses

- Thyroid masses
- Thymic masses
- Germ cell tumors
- Lymph nodes
- Pericardial cyst

Middle mediastinal masses

- Lymph nodes
- Carcinoma of bronchus
- Bronchogenic cyst
- Aneurysm of the aorta

Posterior mediastinal masses

- Neurogenic tumors
- Extramedullary hemopoiesis
- Esophageal masses
- Dilated, ruptured aorta
- Hiatal hernia

Thymic masses

The normal thymus is located anterior to the proximal ascending aorta and superior vena cava (SVC). The gland is bilobed, with the left lobe usually larger than the right (Fig. 1) [46]. It is the largest between the ages of 12 to 19 years and has an attenuation of 30 HU at this stage. Later, fatty involution takes place and the gland is gradually replaced by fat.

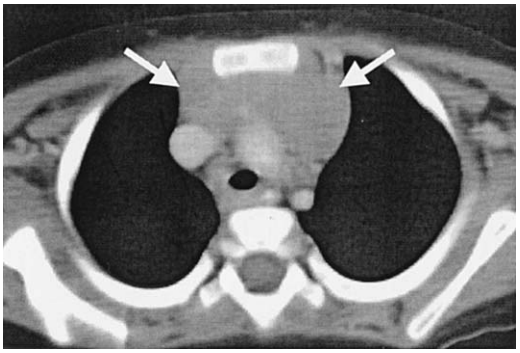

Fig. 1. Normal thymus. Contrast-enhanced CT with mediastinal window settings of a 3-year-old child shows a smooth, well-defined anterior mediastinal structure (*arrows*).

Thymoma

Thymoma is the most common primary tumor of the anterior mediastinum (~20%) [46]. There is a slight female predominance, and the typical presenting age is in the mid-40s. Approximately 30% of patients who have thymoma have myasthenia gravis, and 10% to 15% of all myasthenia gravis patients have thymomas. These thymomas are less aggressive and have a better prognosis. Hematologic disorders such red cell aplasia and hypogammglobulinemia are associated with thymoma. In patients who have myasthenia gravis, CT is indicated even in the absence of pathology on the plain roentgenogram because 25% of thymomas are not apparent on plain radiographs [47,48].

On CT, thymomas usually appear as oval, round, or lobulated masses mostly in the location of the normal thymus, related to the root of the aorta or pulmonary artery. In most cases the contour of the mass is smooth and well defined, and it usually grows asymmetrically to one side of the anterior mediastinum. The mass might be completely or partially outlined by fat or it might replace the anterior mediastinal fat completely. The absence of fat planes between the mass and the mediastinal structures does not necessarily denote the presence of invasion [47]. Homogenous attenuation is common with values of 45 to 75 HU, and mild enhancement is seen following contrast injection [47,49]. Low attenuation areas can represent cyst formation, necrosis, or hemorrhage [46,47,50]. Calcification, even when subtle, can be detected easily by CT [47]. A reliable distinction

between benign and malignant thymoma based on CT characteristics is often impossible. Nevertheless, some CT features are considered to be suspicious of tumor invasion, including heterogeneous mass attenuation, complete obliteration of fat planes, pericardial thickening, encasement of mediastinal vessels, irregular interface with the adjacent lung, and focal or diffuse pleural thickening (Fig. 2) [47,51]. Extension of invasive thymomas into the posterior mediastinum, retrocrural space, and retroperitoneum has been described [51,52].

Treatment consists of surgical excision. Maintaining clear surgical margins is of paramount importance because even noninvasive thymomas can recur if not excised completely.

Lymphoma

Mediastinal lymphadenopathy can be a manifestation of Hodgkin's disease (HD), non-Hodgkin's lymphoma (NHL), infection, metastases, or sarcoidosis (Fig. 3) [2]. Lymphoma accounts for 20% of anterior mediastinal abnormalities in adults and 50% in children. Patients might experience chest pain, dyspnea, dysphagia, shoulder pain, congestive heart failure, hypotension, and SVC syndrome. HD involves the anterior mediastinum or paratracheal region in 90% to 100% of patients. HD typically spreads in contiguous lymph node groups then spreads to the anterior mediastinal compartment [46,53]. Additional thoracic manifestations include pleural or pericardial effusion, sternal erosion, and chest wall erosion. Pulmonary involvement occurs in up to 11% of patients [54]. Low attenuation areas associated with necrosis are seen in 20% to 50% of newly diagnosed cases of HD. The presence of necrotic nodes has no prognostic value [55]. NHL in the chest characteristically involves the middle mediastinum. Extrathoracic disease is also present in 90% of patients. Adenopathy in the cardiophrenic angle is typical for NHL and an unusual site for HD [56].

Lymphoma is treated nonsurgically by chemotherapy and radiotherapy. Calcification can be seen in HD after treatment.

Thyroid masses

Substernal thyroid abnormality is defined as the presence of thyroid tissue below the thoracic inlet.

Goiter

Substernal goiter represents 10% of mediastinal masses. Most thyroid tumors (75–80%) arise from a lower pole or the isthmus and extend into the anterior mediastinum. The remaining 20% to 25% arise from the posterior aspect of each lobe and involve the posterior mediastinum.

Characteristic imaging features include a well-defined mass with a spherical or lobulated border continuous with the thyroid gland in the neck [50]. Thyroid tissue has high density before contrast injection (>100 HU) and undergoes intense immediate and prolonged enhancement after contrast injection. Attenuation of intrathoracic goiter is usually higher than muscle but less than that of the thyroid gland itself. Low-density areas representing cysts or hemorrhage are identified easily on postcontrast scans because they do not enhance, contrary to normal thyroid tissue.

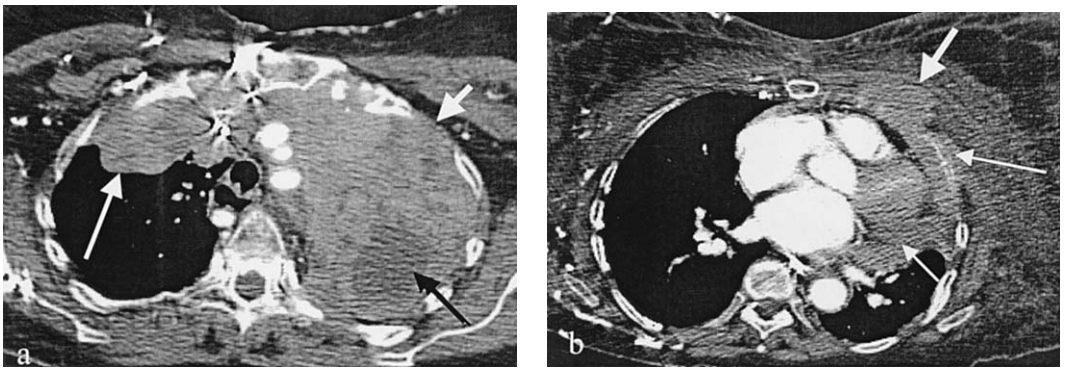

Fig. 2. Invasive thymoma. (*a*) Contrast-enhanced CT with mediastinal window settings demonstrates an extensive heterogenous mass with solid (*short*, *white arrow*) and fluid (*black arrow*) attenuation occupying the left and the right (*long*, *white arrow*) hemithorax. (*b*) Section at the level of the heart demonstrates invasion into the left anterior chest wall, including destruction of the rib cage (*long*, *thin arrow*) and muscle infiltration (*thick arrow*). Also note invasion of the left pericardium (*short*, *thin arrow*). The patient had previously undergone thoracotomy for resection of an invasive thymoma; this is a recurrent tumor.

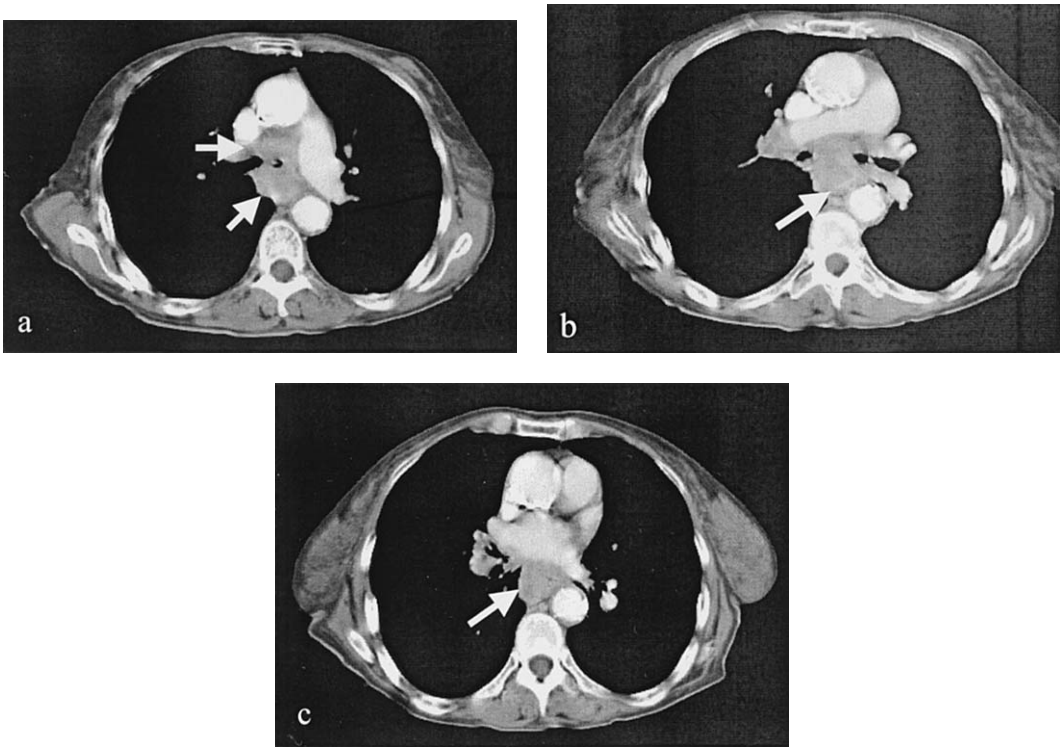

Fig. 3. Mediastinal lymphadenopathy. Contrast-enhanced CT with mediastinal window settings reveals lymphadenopathy in the (*a*) precarinal and retrocarinal regions (*arrows*), (*b*) subcarinal region (*arrow*), and (*c*) azygo–esophageal recess (*arrow*). These lymph nodes have areas of low attenuation caused by necrosis.

Displacement or narrowing of the trachea is typical. Retrotracheal position of the goiter can occur, with splitting of the trachea and the esophagus.

Calcifications are common. Benign calcifications are well defined with a nodular, curvilinear, or circular configuration. Malignant calcifications are usually a group of fine dots corresponding to the psammoma bodies found in papillary and follicular carcinoma of the thyroid [57]. Primary thyroid cancer presents only rarely in the anterior mediastinum, but it can invade it as a direct extension.

Differentiation of benign from malignant thyroid masses on CT is not possible unless obvious invasion beyond the thyroid gland with invasion into the mediastinal fat or chest wall vessels and lymphadenopathy are evident [50,58]. Fine needle aspiration biopsy is not always possible and is rarely reliable for excluding malignancy.

CT is currently the imaging modality of choice for determining the presence and extent of such masses and whether or not impingement on adjacent structures is present. MRI has a limited role (if any) in imaging these masses because of its low sensitivity in detecting calcifications and its high cost [59]. Radionuclide imaging is an accurate method of determining the thyroid nature of an intrathoracic mass. Iodine-131 is the agent of choice, but iodine-123 and Tc-99m are also employed [60]. Proper imaging provides the surgeon with all the relevant information to choose a surgical versus a conservative approach [61].

Germ cell tumors

Germ cell tumors are thought to originate from pluripotent primitive germ cells. They usually occur in the gonads themselves. Extragonadal germ cell tumors are considered to arise from multipotent cells that are misplaced along midline structures during their migration from the urogenital ridge to the primitive gonad [50].

Mediastinal germ cell tumors represent only 1% to 3% of all germ cell neoplasms, and the anterior mediastinum is the most common extragonadal site. These tumors represent 15% of anterior mediastinum tumors in adults and 24% in children [62]. They occur in young adults between the ages of 20 to

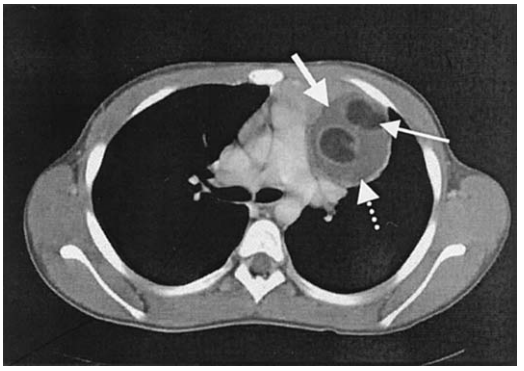

Fig. 4. Teratoma. Contrast-enhanced CT with mediastinal window settings reveals a well-defined, encapsulated (*dotted arrow points to capsule*) anterior mediastinal mass with heterogeneous density consisting of fluid (*thick arrow*) and fat (*thin arrow*).

40 years. Women tend to develop benign tumors, whereas men are prone to developing the malignant germ cell tumors (Fig. 4) [46,63].

Neurogenic tumors

Most neurogenic tumors arise in the paraspinal region, originating in an intercostal or sympathetic nerve. Tumors of neural tissue origin represent 20% of all primary mediastinal tumors in adults and 35% in children [50].

Peripheral nerve tumors

The majority of peripheral nerve tumors arise from an intercostal nerve. Histologic classification includes neurilemoma (schwannoma), neurofibroma (plexiform and nonplexiform types), and neurogenic sarcoma (malignant schwannoma; Fig. 5).

Most peripheral nerve tumors are benign, and complete surgical excision is associated with excellent prognosis. When malignant, these tumors are aggressive and commonly present with metastases, mainly to the lungs [64–66].

Sympathetic ganglia tumors

Tumors of sympathetic ganglia the include ganglioneuroma, ganglioneuroblastoma, and neuroblastoma, a histologic continuum from differentiated benign tissue to frank malignancy. Ganglioneuroma is a benign tumor occurring in children and young adults [65]. Ganglioneuroblastoma includes varying degrees of malignancy and occurs in children younger than 10 years of age. Neuroblastoma is a highly malignant tumor occurring in children younger than 5 years of age, and in this age group a posterior mediastinal mass is considered to be a neuroblastoma until proven otherwise [50]. Vanillymendelic acid, homovanillymendelic acid, and cystathionine are found to be elevated in 90% of patients who have neuroblastomas [65]. Radiographically, they present as elongated, elliptical masses extending over three to five vertebral bodies. The elongated tapering configuration of sympathetic ganglia tumors help distinguish them from other neurogenic tumors. On CT scans they appear well margined with homogeneous or heterogeneous attenuation. Calcifications are demonstrated in 25% of patients. Erosion of the nearby vertebral bodies or ribs is seen more frequently in malignant tumors [67,68]. Neuroblastomas can also show invasion of posterior mediastinal structures and a tendency to cross the midline.

Ganglioneuromas are benign and slow-growing, and surgical excision offers a cure. Neurobalstomas are highly aggressive, presenting as metastatic disease to regional lymph nodes, skeleton, and liver in some patients, in whom 5-year survival does not exceed 30%. The prognosis for ganglioneuroblastoma varies and relates to the patient's age (younger patients show a better outcome), stage, and histologic tumor type [50].

Mediastinal cysts

Cystic masses of the mediastinum are well-defined, round, epithelium-lined masses that contain fluid. Mediastinal cysts represent 15% to 20% of mediastinal masses [21].

Bronchogenic cyst

Bronchogenic cyst is a congenital abnormality caused by ventral budding of the tracheobronchial tree during embryogenesis (Figs. 6). Pseudostratified columnar respiratory epithelium lines these cysts, and cartilage, smooth muscle, and mucous glands are evident in the walls. The content of these cysts is serous fluid or a mixture of mucus and protein. They occur mainly near the carina but can also be found in the middle or posterior mediastinum. Bronchogenic cysts can also be found within the lung parenchyma, pleura, or diaphragm [21]. Other congenital abnormalities such as lobar emphysema, pulmonary sequestration, or a pedicle attaching the cyst to adjacent structures can also be seen. Most patients are asymptomatic, but compression of adjacent structures can cause symptoms such as chest pain, cough, dyspnea, fever, and purulent sputum [20,21]. CT scans demonstrate a round mass with an imperceptible wall. Attenuation values of the cyst content vary from clear fluid to soft tissue attenuation values resulting

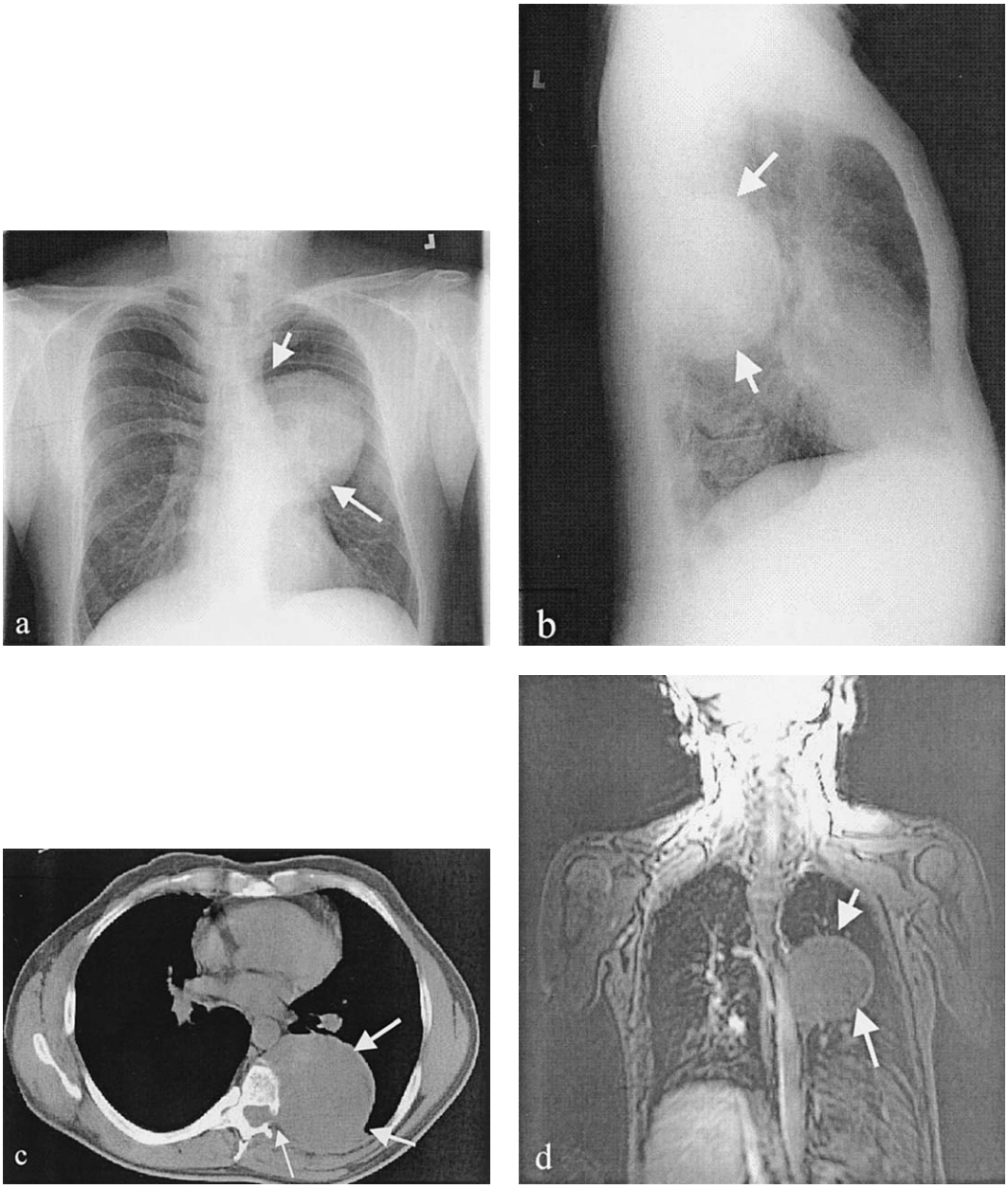

Fig. 5. Malignant peripheral nerve sheath tumor. (*a*) Posterior–anterior chest radiograph demonstrates a spherical mass arising from the mediastinum on the left (*arrows*). (*b*) Lateral chest radiograph confirms that the mass is posterior (*arrows*). (*c*) Non-contrast-enhanced CT with mediastinal window settings shows a large, round mass (*thick arrows*) in the left paraspinal region with scoliosis and enlargement of the neural foramen on this side (*thin arrow*). (*d*) Coronal T1-weighted MRI. A large mass isointense to muscle is noted in the left paraspinal region abutting the vertebral bodies. (*e*) Coronal T1-weighted MRI following gadolinium administration. The aforementioned mass demonstrates heterogeneous enhancement. Scalloping of the left lateral aspects of the midthoracic vertebrae is also seen. Scoliosis curving toward the left side is evident. (Courtesy of Paul Cronin, MD, University of Michigan, Ann Arbor, MI.)

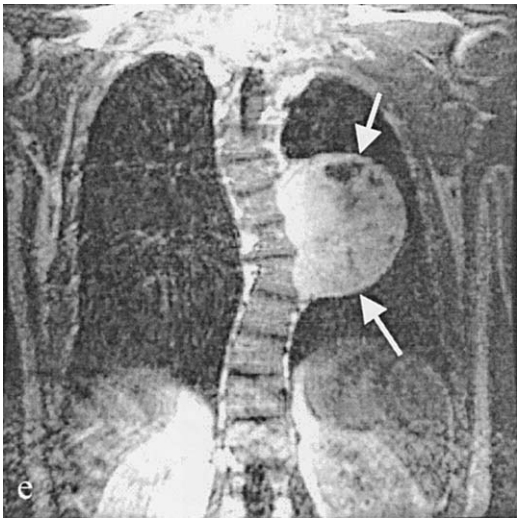

Fig. 5 (*continued*).

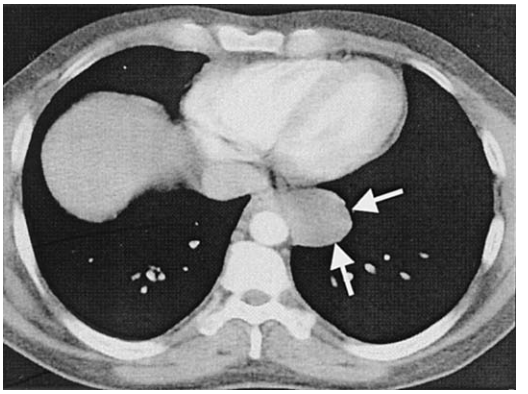

Fig. 7. Neuroenteric cyst. Contrast-enhanced CT with mediastinal window settings shows a posterior mediastinal mass with viscous content measuring 65 HU abutting the descending aorta and esophagus (*arrows*).

from a high content of protein debris or hemorrhage. Cysts containing calcifications have also been described [69].

Surgical excision is indicated in symptomatic patients. Young patients are also advised to remove these cysts because of the low surgical risk and the possibility of complications such as infection, hemorrhage, and neoplasia.

Gastroenteric (neuroenteric) cyst

Esophageal duplication cysts are uncommon. The majority occur within the wall of the esophagus or adjacent to it (see Fig. 7), and they are usually lined entirely or partially by gastric or small intestine mucosa. The term neuroenteric cyst designates the association with spinal column abnormalities [70]. The presence of ectopic gastric mucosa (50% of patients) can cause hemorrhage, perforation, or infection. On CT it resembles a bronchogenic cyst, the only clue being the esophageal proximity or a thicker wall. Patent communication to the gastrointestinal tract is rare when cysts are connected to the esophagus. Upper gastrointestinal barium studies demonstrate extrinsic or intramural esophageal compression [70]. Radionuclide studies with Tc-99 sodium pertechnetate can identify the ectopic gastric mucosa existing in 50% of patients [71]. Neuroenteric cysts demonstrate a fibrous connection to the spine or an intraspinal component [50]. Association with vertebral body anomalies is common. The majority of cysts present in the posterior mediastinum above the level of the carina [21]. CT and MRI characteristics are similar to other foregut cysts. MRI optimally demonstrates the extent and degree of the spinal involvement [72].

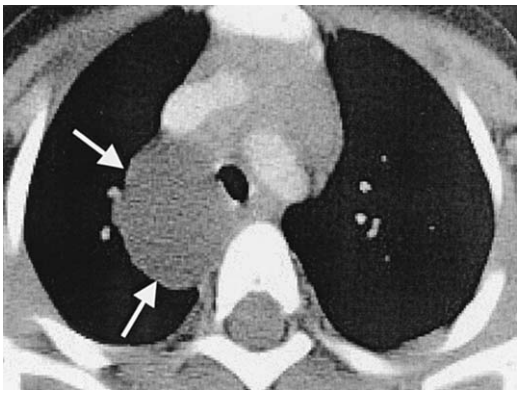

Fig. 6. Bronchogenic cyst. Contrast-enhanced CT with mediastinal window settings shows a well-defined posterior mediastinal mass with clear fluid content and an imperceptible wall (*arrows*). The mass is located adjacent to the trachea.

Pericardial cyst

Pericardial (mesothelial) cysts are a result of aberrations in the formation of coelomic cavities. The cysts usually contain clear fluid and the walls are composed of a single layer of mesothelial cells and connective tissue [21]. The majority of patients are asymptomatic and discovered incidentally. Pericardial cysts vary in size and shape. Seventy percent

of the cysts arise in the right and the remainder in the left cardiophrenic angle or the superior portion of the mediastinum [73]. On CT scans they appear as round–oval cystic masses abutting the pericardium. The benign nature of these lesions can be ascertained by echocardiography, CT, and MRI.

Meningocele

Intrathoracic meningocele results from an abnormal herniation of leptomeninges through either an intervertebral foramen or a vertebral defect. The majority of meningoceles are diagnosed in adults, and association with neurofibromatosis is frequent [74].

CT demonstrates a well-circumscribed, paravertebral, low attenuation mass with distension of the intervertebral foramina and rib anomalies, vertebral anomalies, or scoliosis. When scoliosis is present, the lesion occurs on the convex side [74]. MRI depicts the continuity between the cerebrospinal fluid in the thecal sac and the meningocele [28]. CT myelography following intraspinal injection of contrast can confirm the diagnosis by demonstrating filling of the meningocele [72].

Invasion of mediastinal structures

Malignant primary mediastinal tumors remain a relatively uncommon finding, although their incidence seems to be increasing over the past decades; however, when a malignant mediastinal tumor is present, possible invasion of mediastinal structures has to be determined preoperatively because a decision to resect the mass along with involved neighboring structures must be weighed against the morbidity of such a procedure. In addition, the potential long-term survival benefit must be considered [7].

In general, absolute contraindications to resection of mediastinal masses are invasion of the myocardium or the great vessels and invasion of a long tracheal segment [7]. Overdiagnosis of invasion should be avoided; direct contact between the tumor and mediastinal structures and the absence of cleavage planes are not strictly reliable criteria for predicting invasion. Conversely, clear definition of fat planes surrounding a tumor indicates the absence of macroscopic invasion of adjacent structures [6,12].

Thymomas, germ-cell tumors, lymphomas, and neurogenic tumors account for the vast majority of primary mediastinal tumors in adults. Approximately 30% to 35% of thymomas, 20% of germ-cell tumors, and 15% of nerve sheath tumors are invasive [6,12,14]. Radical excision is the standard of care for invasive thymic tumors and tumors of nerve sheath origin, whereas chemotherapy is the primary treatment modality for invasive germ-cell tumors. A combination of chemotherapy and radiation therapy is required in most cases of lymphoma [7,13,75–77].

In a recent study focused specifically on patients who had malignant mediastinal tumors invading adjacent organs or structures [7], the most commonly invaded structure of the mediastinum was the pericardium, followed by the pleura, the lung (mainly invasion of the anterior segments of the upper lobes or lingula), the phrenic nerve, and the SVC. In cases of massive invasion of the pulmonary hilum or extensive subpleural and pulmonary thymoma metastases, a pneumonectomy cannot be avoided. When clinical SVC syndrome is present and the vein is invaded extensively by the tumor, total SVC replacement is indicated. Widespread collateral venous circulation or extensive thrombosis of subclavian veins increases the likelihood of postoperative thrombosis [7,78].

Invasive thymomas infiltrate adjacent structures including the SVC, great vessels, airways, lungs, and chest wall. An irregular interface with the adjacent lung is suggestive of invasion [47]. There can also be spread to the pericardium and pleura along pleural reflections and along the aorta through the diaphragm into the abdomen and retroperitoneum, usually on one side of the body only (see Fig. 2) [9,12]. It is therefore important, when investigating a potentially invasive thymoma, to include the deep pleural reflections and the upper abdomen on any imaging examination [6,9]. Rarely, thymoma might appear as predominantly pleural disease, usually unilateral, with nonspecific radiographic patterns such as pleural thickening, pleural masses, or diffuse, nodular, circumferential pleural thickening that encases the ipsilateral lung. The latter manifestation mimics malignant mesothelioma or metastatic adenocarcinoma [6,47].

Neural tumors in the posterior mediastinum usually arise close to the spine and can extend through the neural exit foramina into the spinal canal. This intradural extension is not necessarily a sign of malignancy, but it requires a combined neurosurgical and thoracic surgical approach [6,79]. Bone invasion, when present, is a strong indication of malignancy [9].

When a nerve sheath tumor is localized it is not possible to distinguish between benign and malignant tumors [6]. Tumors that grow on intercostal nerves can cause rib erosion. When a sclerotic border is present, the possibility of malignancy is low. Conversely, spreading of multiple ribs with erosion or frank destruction is suggestive of a malignant lesion [6,9].

Vascular supply of mediastinal tumors

The vascular supply of mediastinal tumors depends on their anatomic location, extent, and histopathologic features. In general, congenital mediastinal cysts and the majority of neurogenic tumors are hypovascular lesions, most commonly supplied by the intercostal vessels [13,34,45,79,80]. Anterior intercostal arteries arise from the internal mammary (thoracic) artery and posterior intercostal arteries arise from the thoracic aorta [81]. In each intercostal space there are one posterior and two anterior intercostal veins. The anterior veins drain into the internal mammary veins, the superior four posterior veins drain into the brachiocephalic (innominate) veins, and the lower eight posterior intercostal veins drain into the azygos vein on the right and the accessory hemiazygos and hemiazygos veins on the left [81,82].

Thymomas are supplied by the internal mammary arteries [44], which are located within the adipose and

Table 1
Definition of 1996 American Joint Committee on Cancer/Union Internationale Contre le Cancer classification of regional mediastinal lymph nodes

Number	Name	Location
1	Highest mediastinal nodes	Above a horizontal line at the upper rim of the left brachiocephhalic (innominate) vein where it ascends to the left, crossing in front of the trachea at its midline
2	Upper paratracheal nodes	Above a horizontal line drawn tangential to the upper margin of the aortic arch and below the inferior boundry of number 1 nodes
3A	Prevascular and	Anterior to the aortic arch branches (3A)
3P	Retrotracheal nodes	and posterior to the trachea (3P)
4	Lower paratracheal nodes	On the right: to the right of the midline of the trachea between a horizontal line drawn tangential to the upper margin of the aortic arch and a line extending across the right main bronchus at the upper margin of the right upper lobe bronchus and contained within the mediastinal pleural envelope; azygos nodes are included in this station On the left: to the left of the midline of the trachea between a horizontal line drawn tangential to the upper margin of the aortic arch and a line extending across the left main bronchus at the upper margin of the left upper lobe bronchus medial to the ligamentum arteriosum and contained within the mediastinal pleural envelope
5	Subaortic nodes (aortopulmonary window)	Lateral to the ligamentum arteriosum or the aorta or left pulmonary artery and proximal to the the first branch of the left pulmonary artery and within the mediastinal pleural envelope
6	Paraaortic nodes (ascending aorta or phrenic)	Anterior and lateral to the ascending aorta and the aortic arch or brachiocephalic or the brachiocephalic artery, beneath a line tangential to the upper margin of the aortic arch
7	Subcarinal nodes	Caudad to the tracheal carina but not associated with the lower lobe bronchi or arteries within the lung
8	Paraesophageal nodes	Adjacent to the wall of the esophagus and to the right or left of the midline below the tracheal carina, excluding subcarinal nodes
9	Pulmonary ligament nodes	Within the pulmonary ligament, including those in the posterior wall and lower part of the inferior pulmonary vein
10	Hilar nodes	Proximal to lobar nodes and distal to the mediastinal pleural reflection and the nodes adjacent to the bronchus intermedius on the right

Lymph node stations 1–9 are N2 nodes and lie with the mediasinal pleural envelope. Lymph node station 10 is included in the N1 nodes that are distal to the mediastinal pleural reflection and within the visceral pleura.

connective tissues bordered anteriorly by the costal cartilage and intercostal muscles and posteriorly by the endothoracic fascia and transverse thoracic muscles [83]. Occasionally the arterial supply of thymic tumors can be derived from the inferior thyroid arteries [4]. Venous drainage of the thymic gland is through a variable number of thin vessels (veins of Keynes) that drain the thymus from its posterior surface into the anterior aspect of the left innominate vein. Frequently, one or more veins might join together to form a common trunk before opening into the left innominate vein [4,13,84]. Additionally, one or two small veins from the upper pole of thymus end in the inferior thyroid veins [4].

Intrathoracic goiters receive blood supply from the superior and inferior thyroid arteries. The superior thyroid arteries arise from the external carotids and the inferior thyroid arteries arise from the thyrocervical trunks [4,13,84]. Venous drainage is through the superior, middle, and inferior thyroid veins. The superior and middle thyroid veins end in the internal jugular veins, and the inferior thyroid veins end in the brachiocephalic veins. Sometimes the inferior thyroid veins might join together to form a common trunk ending in the left brachiocephalic vein [4,84].

Since the advent of cisplatin-based chemotherapy, the role of surgery as the primary treatment of germ cell tumors has been more limited [7,75]. Following initial chemotherapy, persistent radiographic abnormalities accompanied by elevated marker levels in the serum that continue to rise denote persistent carcinoma; these patients should be treated with an alternative chemotherapy regimen [75]. Resection of residual masses after chemotherapy has been advocated in patients whose marker levels have normalized [7,75,85–87]. The blood supply of these residual tumors varies according to their size, precise anatomic location, histopathology, and the degree of postchemotherapy necrosis.

Sampling procedures for mediastinal lymph nodes

Lymph nodes are widely distributed throughout the mediastinum. Two systems that have been in used for classifying regional lymph node stations for lung cancer staging were unified in 1996 [88,89]. These were the American Joint Committee on Cancer (AJCC) classification, adapted from the work of Naruke [90], and the classification of the American Thoracic Society and the North American Lung Cancer Study Group [91]. The unified classification was adopted by the AJCC and the Prognostic TNM Committee of the Union Internationale Contre le Cancer. The following discussion of lymph node sampling is according to this unified classification (Table 1).

Surgical procedures used for mediastinal lymph node sampling include cervical mediastinoscopy, anterior mediastinotomy, and video-assisted thoracoscopic surgery (VATS).

Regional lymph nodes accessible by cervical mediastinoscopy include stations 1, 2, 4, and 7 (anterior and superior nodes). When performing anterior or parasternal mediastinoscopy, lymph node stations 5 and 6 can be sampled. VATS offers a panoramic

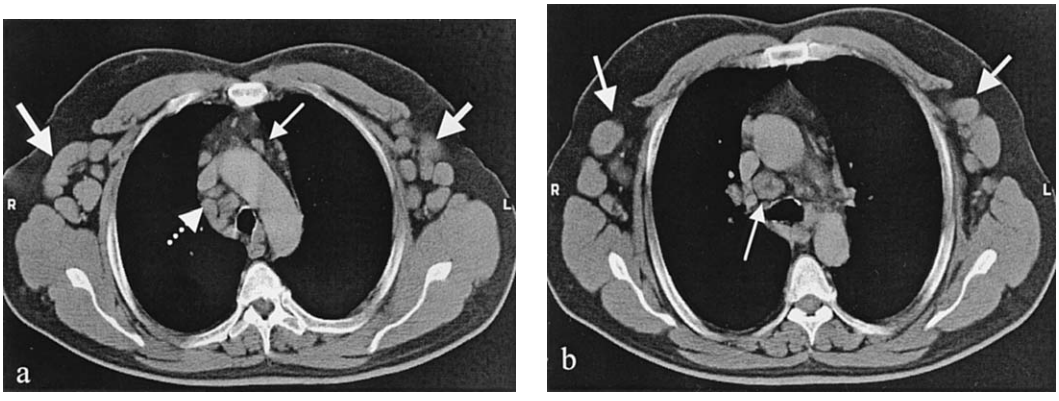

Fig. 8. Mediastinal lymphadenopathy. (*a*) Noncontrast CT with mediastinal window settings demonstrates enlarged lower paratracheal lymph nodes (*dotted arrow*, station 4R) and bilateral axillary lymphadenopathy (*thick arrows*). Small para-aortic lymph nodes are seen on the left (*thin arrow*, station 6). (*b*) Noncontrast CT with mediastinal window settings demonstrates lymphadenopathy further down in the lower paratracheal region (*thin arrow*, station 4R). Lymphadenopathy is noted in both axilla (*thick arrows*).

view of the ipsilateral hemithorax including the hilum, mediastinum, visceral pleura, and chest wall. Lymph node stations accessible by VATS in the right hemithorax include 4R, 9R, and 10R; in the left hemithorax 5, 6, 9L, and 10L are accessible. Right-sided thoracoscopy allows sampling of lymph node stations 3A, 3P, 7 (posterior and inferior nodes), and 8 (Fig. 8) [92].

In studies documenting the size of normal mediastinal lymph nodes by CT, 95% of these lymph nodes were less than 10 mm in diameter [93,94]. The short axis nodal diameter is used for measuring mediastinal lymph nodes because it was found to be the best CT predictor of nodal volume [95]. FDG-PET scanning adds to the accuracy of detecting lymph node involvement in lung cancer staging and has a particularly high negative predictive value [96–98].

Postoperative complications

Postoperative mediastinal complications include mediastinal hemorrhage, mediastinitis, and chylothorax.

Significant hemorrhage can follow thoracic operations, particularly procedures involving the heart and great vessels, which require cardiopulmonary bypass. The clinical presentation is variable and might include retrosternal pain radiating to the back and neck. With increased accumulation of blood in the mediastinum, signs and symptoms related to compression of mediastinal structures, particularly veins, can occur and manifest as dyspnea and cyanosis. With further accumulation of blood, mediastinal tamponade can develop, presenting with circulatory compromise [6,99].

Plain chest radiographs might demonstrate widening of the mediastinal shadow, which can be focal or general. The blood might also track extrapleurally over the lung apices and give rise to apical capping [100]. Severe hemorrhage can rupture into the pleural cavity. Rapid widening of the mediastinum on serial films is an important clue to the diagnosis of mediastinal hemorrhage. CT can show the characteristic appearance of blood, the high density related to a fresh clot, and the relationship of the hematoma to adjacent mediastinal structures (Fig. 9).

Infection of the mediastinum is a relatively rare, serious, and potentially fatal condition that currently occurs most frequently following median sternotomy for open-heart surgery. Postoperative mediastinitis usually occurs between 3 days and 3 weeks following surgery, but delayed manifestations can occur up to months later. The clinical manifestations of mediastinitis are fever, tachycardia, and chest pain, and when it occurs postoperatively there might be wound erythema, pain, effusion, and an unstable sternum [99].

The radiologic features of acute mediastinitis include mediastinal widening and pneumomediastinum. On the lateral chest radiograph, an abnormal soft tissue density, air–fluid levels (representing abscess formation), and sternal dehiscence might be seen. Accompanying pleural effusion on one side or

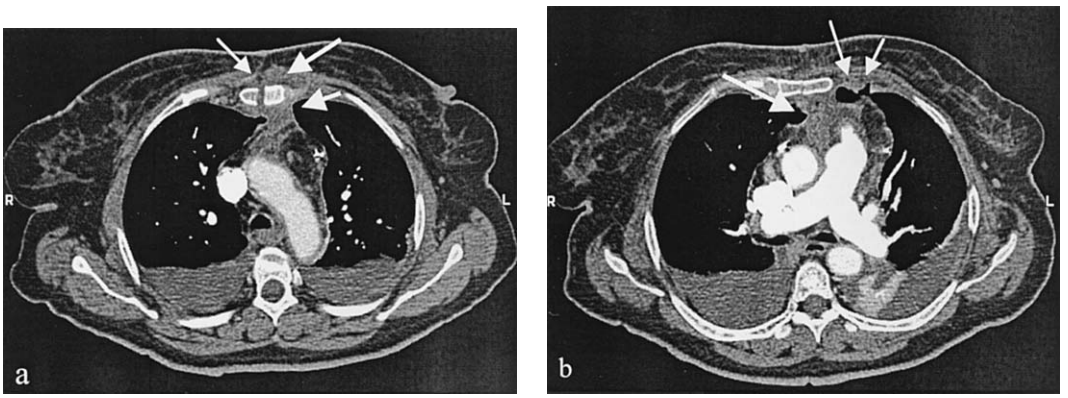

Fig. 9. Postoperative mediastinal hematoma. (*a*) Contrast-enhanced CT with mediastinal window settings demonstrates retrosternal dense fluid collection (*short*, *thick arrow*) measuring 50 HU. Note the sternotomy site (*thin arrow*) and a similar fluid collection anterior to it (*long, thick arrow*). These fluid collections are consistent with postoperative hematomas. Also note the small, bilateral pleural effusions. (*b*) Contrast-enhanced CT with mediastinal window settings. This slice is slightly lower down in the chest. A dense fluid collection is seen anterior to the ascending aorta and the pulmonary trunk, abutting the sternum (*thick arrow*). Two anterior air bubbles are also seen (*thin arrows*), consistent with postoperative air.

bilaterally are common. These findings are recognized more easily on CT scan. CT can also show associated findings such as venous thrombosis or pericardial effusion and contiguous infections such as emphyma, subphrenic abscess, or cervical soft tissue infection [6,99].

Distinguishing retrosternal hematomas from reactive granulation tissue or cellulitis might be difficult, as is differentiating osteomyelitis from postsurgical changes in the sternum. Substernal fluid collections and minimal amounts of air are normal for up to 20 days following sternotomy (Fig. 9). Air can be seen on chest radiographs in the presternal or retrosternal soft tissues for up to 50 days following sternotomy, so only newly appearing air collections or collections that increase in size can be diagnosed as gas-forming infections [101].

Mediastinitis should be diagnosed as early as possible; delays in diagnosing this condition and initiating treatment result in increased morbidity and mortality. Treatment options include incision, debridement and drainage of the involved area, the use of closed irrigation systems, and using a tissue flap (pectoralis or rectus abdominis muscle or omentum) [99].

Chylothorax can develop 1 to 2 weeks following a surgical procedure in the region of the aorta, esophagus, or posterior mediastinum. The anatomy of the thoracic duct is constant only in its variability [102]. The duct originates from the cysterna chili, a globular structure 3 to 4 cm long and 2 to 3 cm in diameter that lies adjacent to the vertebral column between L3 and T10, just to the right of the aorta. Usually a single thoracic duct enters the chest through the aortic hiatus at the level of T12 to T10, just to the right of the aorta. Above the diaphragm the duct lies on the anterior surface of the vertebral column behind the esophagus and between the aorta and the azygos vein. At the level of T5 the duct courses to the left and ascends behind the aortic arch into the left side of the posterior mediastinum, where it passes adjacent to the left side of the esophagus. In the root of the neck, the thoracic duct passes behind the left carotid sheath and jugular vein and enters the venous system at the left jugulo–subclavian junction. There are several anastomoses between the duct and the azygos, intercostals, and lumbar veins. This normal anatomic description exists in slightly more than half of individuals. In the remainder there are two or more main ducts in some part of its course [103].

Injury to the duct has occurred in almost every known thoracic operation. The duct is most vulnerable in the upper part of the left side of the chest, particularly during procedures that involve mobilization of the aortic arch, left subclavian artery, or esophagus. Because of the course of the duct, injury below the level of T5 to T6 usually causes a right-sided chylothorax, whereas injury above this level results in a left-sided chylothorax [103].

There is usually an interval of 2 to 10 days between rupture of the thoracic duct and the onset of a chylous pleural effusion. This delay is caused by the accumulation of lymph in the posterior mediastinum until the mediastinal pleura ruptures [103]. Chylous effusion is typically (but not necessarily) milky, particularly during starvation, as might occur following surgery. The diagnosis of chylous effusion is made by measuring the triglyceride levels of the effusion; levels above 110 mg/dL are regarded as positive. Chylothorax should be differentiated from pseudochylothorax, which is also milky but caused by high levels of cholesterol or lecitin–globulin complexes in the effusion. This condition characteristically occurs in chronic pleural disease with pleural thickening and chronic encysted effusion [104].

A chylous effusion on a plain chest radiograph cannot be distinguished from pleural effusion resulting from other causes. It can be large or small, unilateral or bilateral. On CT, the density of chyle is indistinguishable from that of other effusions despite the high fat content because it is also protein-rich; therefore, the density of the effusion is not as low as would be expected based on the rich fat content [104].

Conservative therapy for chylothorax includes thoracostomy tube drainage, correction of fluid losses, prevention of electrolyte imbalance, and parenteral nutritional support. Surgical therapy is indicated when the chylous effusion does not respond to conservative management and there is no contraindication to surgery. Surgery includes a combination of direct closure of the thoracic duct–pleural fistula, suturing of the leaking mediastinal pleura, and supradiaphragmatic ligation of the duct [103].

Summary

The diagnostic approach to patients who have mediastinal masses should include thorough preoperative imaging. Once limited to plain radiographic techniques, the radiologist now has a wide variety of imaging modalities to aid in the evaluation of the mediastinum. CT is the imaging modality of choice for evaluating a suspected mediastinal mass or a widened mediastinum, and it provides the most useful information for the diagnosis, treatment, and evaluation of postoperative complications.

References

[1] Armstrong P. Normal chest. In: Armstrong P, Wilson AG, Dee P, Hansell DM, editors. Imaging of diseases of the chest. 2nd edition. St. Louis (MO): Mosby; 1995. p. 15–47.

[2] Fraser RS, Paré JAP, Fraser RG, Paré PD. Diseases of the mediastinum. In: Fraser RS, Paré JAP, Fraser RG, Paré PD, editors. Synopsis of diseases of the chest. Philadelphia: WB Saunders; 1994. p. 896–942.

[3] Kohman LJ. Approach to the diagnosis and staging of mediastinal masses. Chest 1993;103:328S–30S.

[4] Williams PL, Warwick R, Dyson M, et al. Gray's anatomy. 37th edition. Edinburgh: Churchill Livingstone; 1989.

[5] Wychulis AR, Payne WS, Clagett OT, Woolner LB. Surgical treatment of mediastinal tumors. A 40-year experience. J Thorac Cardiovasc Surg 1971; 62:379–92.

[6] Armstrong P. Mediastinal and hilar disorders. In: Armstrong P, Wilson AG, Dee P, Hansell DM, editors. Imaging of diseases of the chest. London: Mosby; 2000. p. 789–892.

[7] Bacha EA, Chapelier AR, Macchiarini P, Fadel E, Dartevelle PG. Surgery for invasive primary mediastinal tumors. Ann Thorac Surg 1998;66:234–9.

[8] Shaffer K, Pugatch RD. Diseases of the mediastinum. In: Freundlich IM, Bragg DG, editors. A radiologic approach to diseases of the chest. Baltimore: Williams & Wilkins; 1992. p. 171–85.

[9] Templeton PA. Mediastinal lesions. In: Greene R, Muhm JR, editors. Syllabus: a categorical course in diagnostic radiology. Chest radiology. Oak Brook, IL: Radiological Society of North America Inc; 1992. p. 273–86.

[10] Merten DF. Diagnostic imaging of mediastinal masses in children. AJR 1992;158:825–32.

[11] Pugatch R, Spirn PW. Mediastinal neoplasms. In: Taveras JM, Ferrucci JT, editors. Radiology: diagnosis—imaging—intervention, Vol 1. Philadelphia: Lippincott; 1995.

[12] Naidich DP, Webb WR, Müller NL, Krinsky GA, Zerhouni EA, Siegelman SS. Mediastinum. In: Naidich DP, Webb WR, Müller NL, Krinsky GA, Zerhouni EA, Siegelman SS, editors. Computed tomography and magnetic resonance of the thorax. Philadelphia: Lippincott Williams & Wilkins; 1999. p. 37–159.

[13] Roviaro G, Rebuffat C, Varoli F, Vergani C, Maciocco M, Scalambra SM. Videothroacoscopic excision of mediastinal masses: indications and technique. Ann Thorac Surg 1994;58:1679–84.

[14] Tecce PM, Fishman EK, Kuhlman JE. CT evaluation of the anterior mediastinum: spectrum of disease. Radiographics 1994;14:973–90.

[15] Dedrick CG. Non-neoplastic disorders of the mediastinum. In: Taveras JM, Ferrucci JT, editors. Radiology: diagnosis—imaging—intervention, Vol 1. Philadelphia: Lippincott; 1995.

[16] Glazer HS, Molina PL, Siegel MJ, Sagel SS. Pictorial essay: high-attenuation mediastinal masses on unenhanced CT. AJR 1991;156:45–50.

[17] Glazer HS, Wick MR, Anderson DJ, Semenkovich JW, Molina PL, Siegel MJ, et al. CT of fatty thoracic masses. AJR 1992;159:1181–7.

[18] Gaerte SC, Meyer CA, Winer-Muram HT, Tarver RD, Conces Jr DJ. Fat-containing lesions of the chest. Radiographics 2002;22:S61–78.

[19] Mullins ME, Stein J, Saini SS, Mueller PR. Prevalence of incidental Bochdalek's hernia in a large adult population. AJR 2001;177:363–6.

[20] McAdams HP, Kirejczyk WM, Rosado-de-Christenson ML, Matsumoto S. Bronchogenic cyst: imaging features with clinical and histopathologic correlation. Radiology 2000;217:441–6.

[21] Jeung MY, Gasser B, Gangi A, Bogorin A, Charneau D, Wihlm JM, et al. Imaging of cystic masses of the mediastinum. Radiographics 2002;22:S79–93.

[22] Kawashima A, Fishman EK, Kuhlman JE, Nixon MS. CT of the posterior mediastinal masses. Radiographics 1991;11:1045–67.

[23] Spizarny DL, Rebner M, Gross BH. CT of enhancing mediastinal masses. J Comput Assist Tomogr 1987; 11:990–3.

[24] Doppman JL, Skarulis MC, Chen CC, et al. Parathyroid adenomas in the aortopulmonary window. Radiology 1996;201:456–62.

[25] McAdams HP, Rosado-de-Christenson ML, Moran CA. Mediastinal hemangioma: radiographic and CT features in 4 patients. Radiology 1994;193:399–402.

[26] Kirsch CFE, Webb EM, Webb WR. Multicentric Castleman's disease and POEMS syndrome: CT findings. J Thorac Imaging 1997;12:75–7.

[27] Johnson PT, Fishman EK, Duckwall JR, Calhoun PS, Heath DG. Interactive three-dimensional volume rendering of spiral CT data: current applications in the thorax. Radiographics 1998;18:165–87.

[28] Webb WR, Sostman HD. MR imaging of thoracic disease: clinical uses. Radiology 1992;182:621–30.

[29] Zerhouni EA. MR imaging in chest disease: present status and future applications. In: Green R, Muhm JR, editors. Syllabus: a categorical course in diagnostic radiology. Chest radiology. Oak Brook, IL: Radiological Society of North America Inc; 1992. p. 25–41.

[30] Ho VB, Prince HR. Thoracic MR aortography: imaging techniques and strategies. Radiographics 1998;18: 287–309.

[31] Leung DA, Debatin JF. Three-dimensional contrast-enhanced magnetic resonance angiography of the thoracic vasculature. Eur Radiol 1997;7:981–9.

[32] Wernecke K, Vassallo P, Potte R, Lukener HG, Peters PE. Mediastinal tumors: sensitivity of detection with sonography compared with CT and radiography. Radiology 1990;175:137–43.

[33] Gress FG, Savides TJ, Sandler A, Kesler K, Conces D, Cummings O, et al. Endoscopic ultrasonography, fine-needle aspiration biopsy guided by endoscopic ultrasonography, and computed tomography in the preoperative staging of non–small-cell lung cancer:

a comparative study. Ann Intern Med 1997;127: 604–12.
[34] Cioffi U, Bonavina L, De Simone M, Santambrogio L, Pavoni G, Testori A, et al. Presentation and surgical management of bronchogenic and esophageal duplication cysts in adults. Chest 1998;113:1492–6.
[35] Nguyen BD. Parathyroid imaging with Tc-99m sestamibi planar and SPECT scintigraphy. Radiographics 1999;19:601–14.
[36] Santana L, Givica A, Camacho C. Thymoma. Radiographics 2002;22:S95–102.
[37] Lastoria S, Vergara E, Palmieri G, Acampa W, Varrella P, Caraco C, et al. In vivo detection of malignant thymic masses by indium-111-DTPA-D-Phe1-octreotide scintigraphy. J Nucl Med 1998;39:634–9.
[38] Higuchi T, Taki J, Kinuya S, Yamada M, Kawasuji M, Matsui O, et al. Thymic lesions in patients with myasthenia gravis: characterization with thallium-201 scintigraphy. Radiology 2001;221:201–6.
[39] Waxman AD, Eller D, Ashook G, Ramanna L, Brachman M, Heifetz L, et al. Comparison of gallium-67-citrate and thallium-201 scintigraphy in peripheral and intrathoracic lymphoma. J Nucl Med 1996;37: 46–50.
[40] Fletcher BD, Xiong X, Kauffman WM, Kaste SC, Hudson MM. Hodgkin disease: use of T_1-201 to monitor mediastinal involvement after treatment. Radiology 1998;209:471–5.
[41] Kubota K, Yamada S, Kondo T, Yamada K, Fukuda H, Fujiwara T, et al. PET imaging of primary mediastinal tumors. Br J Cancer 1996;73:882–6.
[42] Sadato N, Tsuchida T, Nakaumra S, Waki A, Uematsu H, Takahashi N, et al. Non-invasive estimation of the net influx constant using the standardized uptake value for quantification of FDG uptake of tumors. Eur J Nucl Med 1998;25:559–64.
[43] Sasaki M, Kuwabara Y, Ichiya Y, Akashi Y, Yoshida T, Nakagawa M, et al. Differential diagnosis of thymic tumors using a combination of 11c-methionine PET and FDG PET. J Nucl Med 1999;40:1595–601.
[44] Landreneau RJ, Dowling RD, Castillo WM, Ferson PF. Thoracoscopic resection of an anterior mediastinal tumor. Ann Thorac Surg 1992;54:142–4.
[45] Sugarbaker DJ. Thoracoscopy in the management of anterior mediastinal masses. Ann Thorac Surg 1993; 56:653–6.
[46] Tecc PM, Fishman EK, Kuhlman JE. CT evaluation of the anterior mediastinum: spectrum of disease. Radiographics 1994;14(5):973–90.
[47] Rosado-de-Christenson ML, Galobardes J, Moran CA. From the archives of the AFIP. Thymoma: radiologic pathologic correlation. Radiograpgics 1992; 12:151–68.
[48] Morgenthaler TI, Brown LR, Clby TV. Thymoma. Mayo Clin Proc 1993;68:110–1123.
[49] Santana L, Givica A, Camacho C. Best cases from the AFIP thymoma. Radiograhpics 2002;22:S95–102.
[50] Fraser RS, Muller N, Colman N, Pare PD. Mediastinal disease. In: Fraser RS, Muller N, Colman N, Pare PD, editors. Fraser and Pare's diagnosis of diseases of the chest. Philadelphia: Saunders; 1999. p. 2875–974.
[51] Zerhouni EA, Scott WW, Baker RR. Invasive thymomas: diagnosis and evaluation by computed tomography. J Coput Assist Tomogr 1982;6:92.
[52] Scatarige JC, Fishman EK, Zerhouni EA. Transdiaphragmatic extension of invasive thymoma. AJR 1985;144:31.
[53] Diehl L, Hopper K, Giguere J, Garnger E, Lesar M. The pattern of intrathoracic Hodgkin's disease assessed by computed tomography. J Clin Oncol 1991; 9:438–43.
[54] Guermazi A, Brice P, de Kerviler E, Fermé C, Hennequin C, Meignin V, et al. Extranodal Hodgkin disease: spectrum of disease. Radiographics 2001;21: 161–79.
[55] Salonen O, Kivisaari L, Somer K. Differential diagnosis of anterior upper mediastinal expansions by contrast-enhanced computed tomography. Comut Radiol 1984;8:217–22.
[56] Filly R, Blank N, Castellino R. Radiographic distribution of intrathoracic disease in previously untreated patients with Hodgkin's disease and non Hodgkin's lymphoma. Radiology 1976;120:277–81.
[57] Kowolafe F. Radiological patterns and significance of thyroid calcifications. Clin Radiol 1981;32:571–5.
[58] Takashima S, Morimoto S, Ikezoe J. CT evaluation of anaplastic thyroid carcinoma. AJR 1990;154:1079.
[59] Jennings A. Evaluation of substernal goiters using computed tomography and MR imaging. Endocrinol Metab Clin N Am 2001;30(2):401–14.
[60] Park HM, Traver RD, Siddiqui AR. Efficacy of thyroid scintigraphy in the diagnosis of intrathoracic goiter. AJR 1987;148:527.
[61] Sanders LE, Rossi RL, Shahian DM, Willamson WA. Medaistinal goiters. The need for an aggressive approach. Arch Surg 1992;127(5):609–13.
[62] Rosado-de-Christenson ML, Tempelton PA, Moran CA. From the archives of the AFIP—mediastinal germ cell tumors: radiologic pathologic correlation. Radiogarphics 1992;12:1013–30.
[63] Nichols CR. Mediastinal germ cell tumors: clinical features and biologic correlates. Chest 1991;99: 472–9.
[64] Wood DE. Mediastinal germ cell tumors. Semin Thorac Cardiovasc Surg 2000;12(4):278–89.
[65] Gale AW, Jelihovsky T, Grant AF. Neurogenic tumors of the mediastinum. Ann Thorac Surg 1974; 17:434.
[66] Kawashima A, Fishman EK, Kuhlman J, Nixon M. CT of posterior mediastinal masses. Radiographics 1991;11:1045–67.
[67] Bourgouin PM, Shepard JO, Moore EH. Plexiform neurofibromatosis of the mediastinum: CT appearance. AJR 1992;159:279.
[68] Reed JC, Kagan-Hallett K, Feigin DS. Neural tumors of the thorax: subject review from the AFIP. Radiology 1978;126:9.
[69] Mendelson DS, Rose SJ, Efermidis SC, Kirschner

PA, Cohen BA. Bronchogenic cysts with high CT numbers. AJR 1983;140:463–5.
[70] Azzie G, Beasley S. Diagnosis and treatment of foregut duplications. Semin Pediatr Surg 2003;12(1): 46–54.
[71] Salo JA, Ala-Kulju K. Congenital esophageal cyst in adults. Ann Thorac Surg 1987;44:135–8.
[72] Erasmus JJ, Mcadams HP, Donnelly LF, Spritzer CE. MR imaging of mediastinal masses. Magn Reson Imaging Clin N Am 2000;8(1):59–89.
[73] Feigin DS, Fenoglio JJ, Mcalsiter HA, Medawell JE. Pericardial cysts: a radiographic pathologic correlation and review. Radiology 1977;25:15–20.
[74] Aughenbaugh GL. Thoracic manifestations of neurocutaneous diseases. Radiol Clin N Am 1984;22: 741–56.
[75] Kantoff P. Surgical and medical management of germ cell tumors of the chest. Chest 1993;103:331S–3S.
[76] Costello P. Chest lymphoma. In: Greene R, Muhm JR, editors. Syllabus: a categorical course in diagnostic radiology: Chest radiology. Oak Brook, IL: Radiological Society of North America Inc; 1992. p. 245–58.
[77] Gawrychowski J, Rokicki M, Gabriel A. Thymoma the usefulness of some prognostic factors for diagnosis and surgical treatment. Eur J Surg Oncol 2000;26: 203–8.
[78] Dartavelle PG, Chapelier AR, Pastorino U, Corbi P, Lenot B, Cerrina J, et al. Long-term follow-up after prosthetic replacement of the superior vena cava combined with resection of mediastinal–pulmonary malignant tumors. J Thorac Cardiovasc Surg 1991;102: 259–65.
[79] Naunheim KS. Video throacoscopy for masses of the posterior mediastinum. Ann Thorac Surg 1993;56: 657–8.
[80] Demmy TL, Krasna MJ, Detterbeck FC, Kline GG, Kohman LJ, DeCamp Jr MM, et al. Multicenter VATS experience with mediastinal tumors. Ann Thorac Surg 1998;66:187–92.
[81] Sobotta J. In: Ferner H, Staubesant J, editors. Atlas der anatomie des menschen [atlas of human anatomy], Vol. 2. Munich: Uran-Schwarzenberg; 1972. p. 27–39 [in German].
[82] Lawler LP, Corl FM, Fishman EK. Multi-detector row and volume-rendered CT of the normal and accessory flow pathways of the thoracic systemic and pulmonary veins. Radiographics 2002;22:S45–60.
[83] Kuzo RS, Ben-Ami TE, Yousefzadeh DK, Ramirez JG. Internal mammary compartment: window to the mediastinum. Radiology 1995;195:187–92.
[84] DeCamp Jr MM, Swanson SJ, Sugarbaker DJ. The mediastinum. In: Baue AE, Geha AS, Hammond GL, et al, editors. Glenn's thoracic and cardiovascular surgery. 6th edition. Stanford: Appleton & Lange; 1996. p. 643–63.
[85] Toner GC, Panicek DM, Heelan RT, Geller NL, Lin SY, Bajorin D, et al. Adjunctive surgery after chemotherapy for nonseminomatous germ cell tumors: recommendations for patients selection. J Clin Oncol 1990;8:1683–94.
[86] Nichols CR, Saxman S, Williams SD, Loehrer PJ, Miller ME, Wright C, et al. Primary mediastinal nonseminomatous germ cell tumors: a modern single institution experience. Cancer 1990;65:1641–6.
[87] Wright CD, Kesler KA, Nichols CR, Mahomed Y, Einhorn LH, Miller ME, et al. Primary mediastinal nonseminomatous germ cell tumors. Results of a multimodality approach. J Thorac Cardiovasc Surg 1990;99:210–7.
[88] Mountain CF, Dresler CM. Regional lung cancer classification for lung cancer staging. Regional lymph node classification in lung cancer staging. Chest 1997;111:1718–23.
[89] Mountain CF. Revisions in the international system for staging lung cancer. Chest 1997;111:1710–7.
[90] American Joint Committee on Cancer. Lung. In: Beahrs OH, Henson DE, Hutter RVP, et al, editors. Manual for staging cancer. 4th edition. Philadelphia: Lippincott; 1992. p. 115–21.
[91] American Thoracic Society. Medical section of the American Lung Association. Clinical staging of primary lung cancer. Am Rev Respir Dis 1983;127: 659–64.
[92] Cymbalista M, Waysberg A, Zacharias C, Ajavon Y, Riquet M, Rebibo G, et al. Demonstration of the 1996 AJCC-UICC regional lymph node classification for lung cancer staging. Radiographics 1999; 19:899–900.
[93] Genereux GP, Howie JL. Normal mediastinal lymph node size and number: CT and anatomic study. AJR Am J Roentgenol 1984;142(6):1095–100.
[94] Quint LE, Glazer GM, Orringer MB, Francis IR, Bookstein FL. Mediastinal lymph node detection and sizing at CT and autopsy. AJR Am J Roentgenol 1986;147(3):469–72.
[95] Glazer GM, Gross BH, Quint LE, Francis IR, Bookstein FL, Orringer MB. Normal mediastinal lymph nodes: number and size according to American Thoracic Society mapping. AJR Am J Roentgenol 1985;144(2):261–5.
[96] Graeter TP, Hellwig D, Hoffmann K, Ukena D, Kirsch CM, Schafers HJ. Mediastinal lymph node staging in suspected lung cancer: comparison of positron emission tomography with F-18-fluorodeoxyglucose and mediastinoscopy. Ann Thorac Surg 2003;75(1):231–5 [discussion 235–6].
[97] von Haag DW, Follette DM, Roberts PF, Shelton D, Segel LD, Taylor TM. Advantages of positron emission tomography over computed tomography in mediastinal staging of non-small cell lung cancer. J Surg Res 2002;103(2):160–4.
[98] Kernstine KH, Mclaughlin KA, Menda Y, Rossi NP, Kahn DJ, Bushnell DL, et al. Can FDG-PET reduce the need for mediastinoscopy in potentially respectable nonsmall cell lung cancer? Ann Thorac Surg 2002;73(2):394–401 [discussion 401–2].
[99] Davis RD, Oldham HN, Sabiston DC. The mediasti-

num. In: Sabiston DC, Spencer FC, editors. Surgery of the chest. 6th edition. Philadelphia: WB Saunders; 1995. p. 576–611.

[100] Simeone JF, Minagi H, Putman CE. Traumatic disruption of the thoracic aorta: significance of the left apical extrapleural cap. Radiology 1975;117: 265–8.

[101] Carter AR, Sostman HD, Curtis AM, Swett HA. Thoracic alterations after cardiac surgery. AJR Am J Roentgenol 1983;140:475–81.

[102] Davis HK. A statistical study of the thoracic duct in man. Am J Anat 1915;17:211.

[103] Cohen RG, DeMeester TR, Lafontaine E. The pleura. In: Sabiston DC, Spencer FC, editors. Surgery of the chest. 6th edition. Philadelphia: WB Saunders; 1995. p. 523–75.

[104] Wilson AG. Pleura and pleural disorders. In: Armstrong P, Wilson AG, Dee P, Hansell DM, editors. Imaging of diseases of the chest. 2nd edition. St. Louis (MO): Mosby; 1995. p. 641–716.